Neutron Scattering Analysis of the *Cryptococcus neoformans* Polysaccharide Reveals Solution Rigidity and Repeating Fractal-like Structural Patterns

Ziwei Wang[1], *Susana C. M. Teixeira*[2,3,*], *Camilla Strother*[1], *Anthony Bowen*[1], *Arturo Casadevall*[1], *and Radamés JB Cordero*[1,*]

[1]Department of Molecular Microbiology and Immunology, Johns Hopkins Bloomberg School of Public Health, Baltimore, Maryland, 21205, USA

[2]NIST Center of Neutron Research, National Institute of Standards and Technology, Gaithersburg, Maryland, 20899, USA

[3]Department of Chemical and Biomolecular Engineering, University of Delaware, Newark, Delaware, 19716, USA

KEYWORDS: *Cryptococcus*, extracellular polysaccharide, neutron scattering, glucuronoxylomannan, mass fractal, fungal pathogen

ABSTRACT: *Cryptococcus neoformans* is a fungal pathogen that can cause life-threatening brain infections in immunocompromised individuals. Unlike other fungal pathogens, it possesses a protective polysaccharide capsule crucial for its virulence. During infections, *Cryptococcus* cells release copious amounts of extracellular polysaccharides (exo-PS) that interfere with host immune responses. Both exo-PS and capsular-PS are pivotal in *Cryptococcus* infections and represent key targets for disease diagnosis and vaccine development strategies. However, understanding their structure is complicated by their polydispersity, complexity, sensitivity to sample isolation and processing and scarcity of methods capable of isolating and analyzing them while preserving their native structure. In this study, we employ small-angle neutron scattering (SANS) and ultra-small angle neutron scattering (USANS) for the first time to investigate both fungal cell suspensions and extracellular polysaccharides in solution. Our data suggests that exo-PS in solution exhibits collapsed chain-like behavior and mass fractal properties that imply a repeating pattern or structure that recurs at different levels of magnification. The local structure of the polysaccharide is characterized as a rigid rod on a scale-length that corresponds to 3 to 4 repeating units. This research not only unveils insights into exo-PS and capsular-PS structures but also demonstrates the potential of USANS for studying changes in cell dimensions and the promise of contrast variation in future neutron scattering studies.

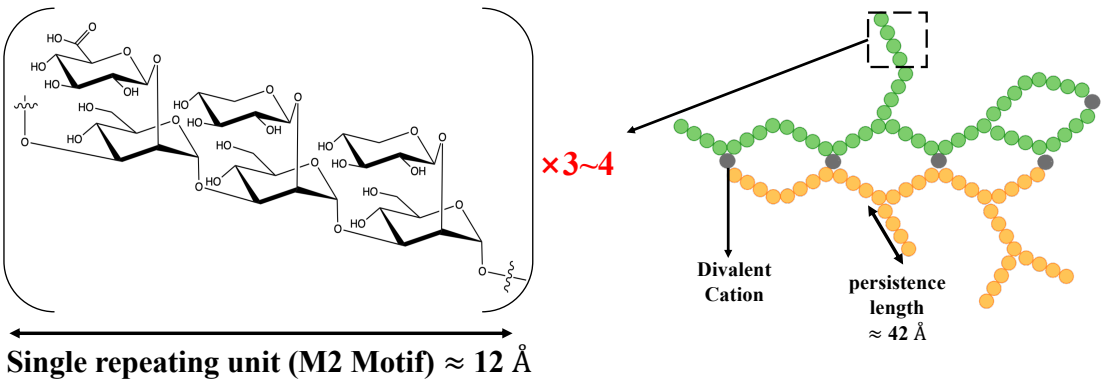

INTRODUCTION

Cryptococcal meningitis is a deadly fungal infection caused by *Cryptococcus neoformans,* one of the leading causes of death in HIV/AIDS patients in sub-Saharan Africa[1,2]. Within brain tissues, the fungus secretes copious amounts of polysaccharide (exo-PS) to the cerebrospinal fluid, believed to cause elevated intracranial pressure and disruption of an effective immune response[2,3]. The fungal cell is encased by a thick capsule composed of polysaccharide (capsular-PS), which protects from the host's immune defense mechanisms[4]. Both the exo-PS and capsular-PS are mainly comprised of glucuronoxylomannan (GXM), which is formed by an α-1,3-linked mannan backbone with β-1,2- and/or β-1,4-linked glucuronyl and xylosyl units that contribute to serological diversity. GXM molecules are assembled from six structural units (M1-6), referred to as triads, featuring a glucuronic acid residue every third mannose along with varying xylose substitutions (**Figure 1**). Due to its high water content (over 95% of total mass and volume), the PS capsule is highly susceptible to dehydration steps employed in high-resolution microscopy or lyophilization, which disturb the native structure[5,6].

C. neoformans exo-PS and capsular-PS are key virulence determinants and targets for the immune system, vaccine design, and monoclonal antibody (mAb) treatments. Diagnosis of *Cryptococcus* infection primarily relies on antibody-based methods[7,8]. Although both exo-PS and capsular-PS are predominantly composed of GXM, they exhibit distinct physicochemical properties and mAb reactivity[8]. Despite their significance in disease and diagnosis, the epitope structures recognized by these antibodies remain unknown. Understanding the PS structure is therefore crucial for the design of diagnostic assays and strategies for vaccine development.

The large and complex PS heteropolymers display physicochemical characteristics that vary based on nutrient availability, chemical and physical environment, and cell age[8,9]. Consequently,

experimental biases can be introduced by sample preparation protocols and the inherent limitations of measurement techniques. Previous research has primarily focused on PS isolated from culture supernatants using hexadecyltrimethylammonium bromide (CTAB) precipitation or filtration, and capsular-PS extracted via dimethylsulfoxide (DMSO) extraction and ionizing radiation-induced PS ablation, leading to nominally de-capsulated cells (though residual capsular-PS may remain). A variety of techniques, such as static (SLS) and dynamic light scattering (DLS), zeta potential measurements, optical tweezers-based elastic modulus assessments, and solution viscosity analyses, have been employed to investigate exo-PS and capsular-PS structure[10,11]. SLS and DLS analyses suggest that the polysaccharide molecules are branched, a characteristic that influences immune reactivity and modulation[12–15]. Existing experimental data is consistent with capsular-PS polymers in molar mass ranges of 1-7 MDa, radii of gyration (R_g) ranging from 150-500 nm, hydrodynamic radii (R_h) ranging spanning 570-2000 nm, contingent on the specific experimental method used[10,13,16,17]. Encapsulated and nominally de-capsulated cells were previously investigated by powder X-ray diffraction, where broad peaks with the range of 1.46-1.51 $Å^{-1}$ for relatively large momentum transfer vector q magnitudes, were attributed to a repeating structural motif arising from inter-molecular interactions mediated by divalent metals, glucuronic acid residues, and/or possibly gelated PS organization[18]. A detailed characterization of the relationship between the structures of exo-PS and capsular-PS, and their corresponding functions at different stages of infection, requires measurement capabilities that preserve PS conformation.

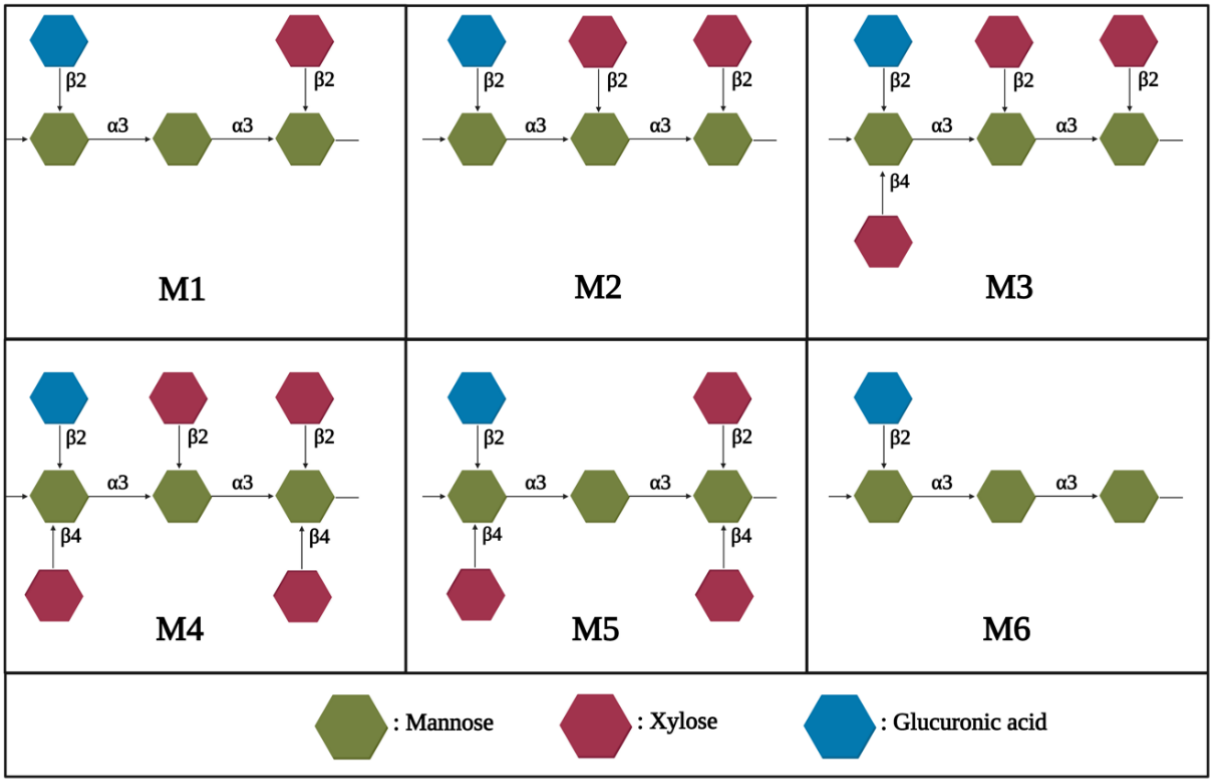

Figure 1. The six Glucuronoxylomannans (GXM) motifs that build up fungal exo-PS and capsular-PS. GXM is composed of a combination of six repeating units (M1-6), defined by a glucuronic acid (GlcA) residue every 3rd mannose with varying xylose substitutions. These 6 motifs of GXM in various combinations correlate to different serotype activities[19]. *C. neoformans* H99 serotype A has a dominant M2 motif in exo- and capsular-PS[20]. Polysaccharide molecules can be heteropolymers composed of more than one triad[17]. Image created with BioRender.com.

In this study, we used neutron scattering analyses to probe the structure of exo-PS, intact fungal cells, and gamma-irradiated nominally de-capsulated cells in solution (**Figure 2**). Neutron scattering offers access to a broad range of structural features without causing radiation damage, enabling data collection on the same samples across small-angle (SANS) and ultra-small angle

(USANS) neutron scattering regimes at various temperatures and concentrations. This approach minimizes sample discrepancies, while the use of varying percentages of D_2O in buffers allows for contrast variation. Given the considerable size of the cells (micrometers in diameter), the USANS regime is crucial, whereas the analysis of intrachain structures is conducted within the SANS regime.

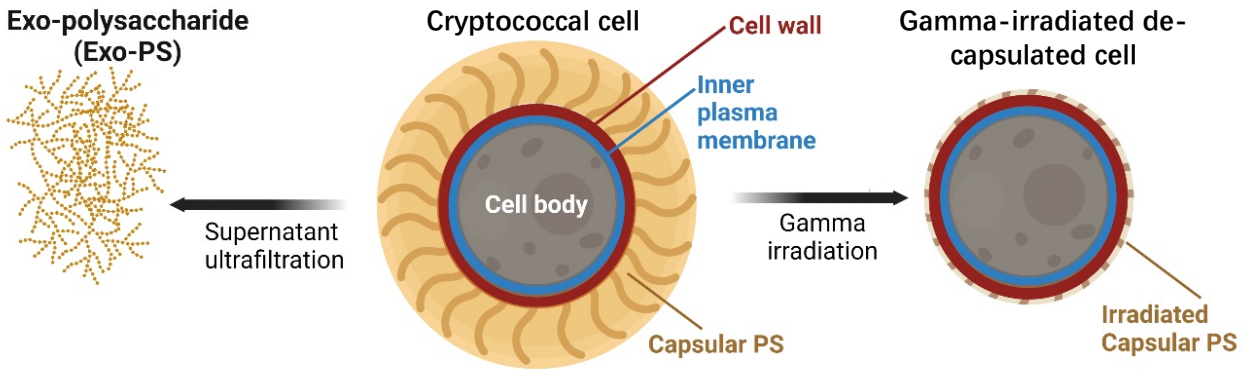

Figure 2. Schematic diagram of the samples investigated: exo-PS, cryptococcal cell, and gamma-irradiated de-capsulated cell. Exo-PS refers to the secreted polysaccharide, while capsular-PS refers to the highly hydrated polysaccharide surrounding the capsule of the intact cell. Gamma-irradiated capsular-PS refers to the remaining polysaccharide thin capsule surrounding the irradiated cells. Image created with BioRender.com.

MATERIALS AND METHODS

Fungal Growth. *Cryptococcus neoformans* Serotype A strain H99 was inoculated in 20 mL of Sabouraud dextrose broth and grown with agitation (120 rpm) for 2 days at 30 °C. The cells were pelleted by centrifuging for 10 minutes at 3000 rpm, and resuspended in minimal media (15 mM dextrose, 10 mM $MgSO_4$, 29.3 mM KH_2PO_4, 13 mM glycine, and 3 μM thiamine-HCl, adjusted to pH 5.5 using KOH). The washing process was repeated three times, and the cells were finally resuspended in minimal media to a density of 1×10^6 cells/mL. Subsequently, the cells were inoculated into a 1 L culture of minimal media and incubated at 30 °C for 7 days. The cells were harvested via centrifugation at 4,000 rpm for 20 minutes. The supernatant was filtered using a 0.22 μm Millipore.

Capsular-PS was removed by exposing the whole cells to 40 minutes of gamma irradiation, using the method demonstrated by Maxson *et al.* [21]. The ionizing radiation was demonstrated to be effective in removing the capsular-PS [22].

Exo-PS Isolation. The exo-PS was isolated from the cell-free supernatant as previously described[23]. The supernatant was sequentially filtered with an Amicon membrane filter (100 kDa nominal molar mass cutoff) and the flow-through was then filtered using a 10 kDa membrane filter. The exo-PS accumulated on the 10 kDa membrane surface as a clear gel and was collected and dialyzed extensively against MilliQ-grade H_2O or D_2O (Cambridge Isotope Labs, 99.9% D). The H_2O solutions provide scattering profiles at an additional contrast, while the samples prepared in D_2O are expected to minimize the incoherent neutron scattering background contribution to the measured intensity profiles. Following dialysis, the exo-PS concentration was determined using a phenol sulfuric colorimetry assay[24]. Sample solutions were centrifuged for 2 minutes at 10,000 rpm

to remove any debris. This process resulted in 10mg/mL exo-PS samples with a hydrodynamic radius R_h of 550-600 nm and relatively low polydispersity, quantified as 0.355 (**Figure S1**) by DLS coupled with a 90Plus/BI-MAS Multi-Angle Particle Sizing analyzer (Brookhaven Instruments Corp., NY, USA), as described by Frases *et al.*[16]. The prepared exo-PS was also resuspended at 1 mg/mL and 5 mg/mL. The polymer overlap concentration c^* for polysaccharides and well-hydrated polymers is typically reported in the 7-10 mg/mL range[23–26].

SANS and USANS Data Collection and Reduction. Neutron scattering data were collected at the National Institute of Standards and Technology (NIST) Center for Neutron Research (NCNR; Gaithersburg, Maryland USA). All samples were degassed for 10 minutes before data collection. SANS data were obtained from the 30-meter instruments NG7 and NGB, using a neutron wavelength λ of 6 Å and a wavelength spread $\Delta\lambda/\lambda$ of 12.5 % for three sample-to-detector distances, to measure scattered intensities over a range of momentum transfer defined as:

$$q = \frac{4\pi \sin\theta}{\lambda} \quad (1)$$

where 2θ is the scattering angle measured. Focusing lenses were used for the longer wavelengths (8.4 Å on NGB, and 8.09 Å on NG7) to extend the lower q range to 0.001 $Å^{-1}$ in the SANS regime[29]. Scattered neutrons were detected with a 64 cm × 64 cm 2D position-sensitive detector with 128 pixels × 128 pixels at a resolution of 0.508 cm/pixel. SANS data measured for solutions in H_2O at concentrations of exo-PS up to 10 mg/mL show a flat intensity profile in the q range measured, indicative of insufficient contrast to provide a measurable signal above the strong incoherent scattering background from the hydrogen atoms in the buffer (**Figure S2**). SANS measurements were carried out on 1 mg/mL, 5 mg/mL, and 10 mg/mL of exo-PS solutions in D_2O at three temperatures (22 °C, 30 °C, and 37 °C), controlled by a Peltier-driven sample changer, with 30

minutes of pre-equilibration at the desired temperature before data collection. The temperatures chosen include typical ambient experimental environments (22 °C), as well as the *C. neoformans* optimal growth (30 °C), and physiological temperatures (37 °C). No significant differences were observed between the SANS profiles of exo-PS solutions at the three measured temperatures (data not shown): the profiles overlapped well, within experimental error. A temperature of 30 °C was therefore chosen for data collection on the whole cells and gamma-irradiated cells in the SANS and USANS regime, for consistency with the growth temperature of the whole fungal cells.

Slit-smeared USANS data were collected at the double-crystal diffractometer (Bonse-Hart) BT5[30]. at the NCNR (λ = 2.4 Å, $\Delta\lambda/\lambda$ = 6%), to cover a q range of 0.00003 Å^{-1} to 0.003 Å^{-1}. USANS measurements were carried out on 10 mg/mL exo-PS in D_2O at 30 °C to probe the presence of aggregates or finite size clusters or aggregates in the micrometer to hundreds of nanometers size range. USANS data were also collected on D_2O and H_2O solutions of the whole fungal cells, and gamma irradiated cells at the concentration of 1×10^8 cells/mL.

SANS and USANS data were reduced using the macro-routines developed for IGOR Pro at the NCNR[31]. Raw counts were normalized to a common neutron monitor count and corrected for empty cell counts, ambient background counts, and nonuniform detector response. The data obtained from the samples were placed on an absolute scale by normalizing the scattered intensity to the incident beam flux. Buffer-only reduced data were subtracted from SANS data on samples containing exo-PS or capsular-PS.

Neutron Scattering Data Fitting. The SANS data for the exo-PS solutions in D_2O were fitted using a modified empirical correlation length function that calculates scattering intensities as:

$$I(q) = \frac{A}{q^n} + \frac{C}{1 + (q\xi)^m} + B \quad (2)$$

where the first term describes Porod scattering from clusters (exponent n) and the second term is a Lorentzian function describing scattering from the PS polymer chains (exponent m)[32]. The second term characterizes the PS/solvent interactions, and the two multiplicative factors A and C are, respectively, the Porod scale and the Lorentz scale. ξ is a correlation length for the PS chains, and B is a q-independent incoherent neutron scattering intensity background contribution to I(q). The calculated intensities from the correlation length model were smeared to match the instrumental pinhole smearing read from the reduced experimental data file. The exo-PS volume fraction and the B parameter were kept fixed throughout the fits. The fitting parameters and relevant information on the goodness-of-fit are available in the supplementary material for the interested reader (**Table S1**). It was assumed that the entanglement of overlapping PS chains did not contribute significantly towards the SANS profiles: this assumption is discussed in the results section.

Light Microscopy. To measure the cell and capsule dimensions, whole cells and gamma-irradiated cells in D_2O and H_2O at 1×10^8 cells/mL were imaged with an Olympus AX70 microscope, using the QCapture Suite V2.46 software for Windows. Cryptococcal cells were suspended in India Ink, which is excluded by the PS so that the capsule region will appear to be bright/empty. Cell dimensions were measured with ImageJ in pixels, and then converted to μm (152 pixels correspond to 50 μm for 40× magnification objective with 2×2 binning). Statistical analyses were performed using GraphPad Prism version 9.5.1 for Mac OS X, GraphPad Software, Boston, Massachusetts USA. Unpaired statistical analyses t-tests were done for the cell diameters

and capsule thickness comparisons; the corresponding significance was stratified based on the probability that the results occur by chance, quantified as a probability through a percentage p-value, where 5% is equivalent to $p = 0.05$.

Scanning Electron Microscopy. SEM of encapsulated *C. neoformans* yeast cells was done as previously described[13]. Briefly, the cells were fixed using a solution containing glutaraldehyde, sodium Cacodylate, sucrose, and $MgCl_2$. After dehydration with ethanol, critical point drying was performed using liquid carbon dioxide. The dried samples were then sputter-coated with gold-palladium for improved conductivity. Finally, the prepared samples were visualized using a JEOL JSM6400 Scanning Electron Microscope at an accelerating voltage of 10 KV, enabling high-resolution imaging of the yeast cells. To analyze the fractal dimension of SEM images of whole cells and capsular-PS structures, we utilized the FracLac plugin of ImageJ (http://rsb.info.nih.gov/ij/plugins/fraclac/FLHelp/Introduction.htm). The FracLac algorithm quantifies the complexity of patterns in digital images, providing fractal dimensions data. The algorithm works by scanning the input micrographs using a shifting grid algorithm, which allows multiple scans from different locations on each image.

RESULTS AND DISCUSSION

SANS Analysis of Exo-PS Solutions. Based solely on the water-free composition, the neutron scattering length density (SLD) of polysaccharides in H_2O is expected to range from 1×10^{-6} Å^{-2} to 2×10^{-6} Å^{-2} (the SLD of pure H_2O is -0.56×10^{-6} Å^{-2})[33]. The flat scattering profiles observed in the exo-PS samples are consistent with their high hydration state and a significant contribution of incoherent scattering originating from the hydrogen atoms within the samples (**Figure S2**). In the case of exo-PS solutions in D_2O, there is still a relatively strong incoherent neutron scattering background observed in the reduced SANS data due to the hydrogen atoms (**Figure 3**). The predominant M2 motif expected in our sample consists of three mannoses, two xyloses, and one glucuronic acid[20], containing a significant number of labile hydrogens that can exchange against D_2O during dialysis. However, non-labile and solvent-inaccessible hydrogen atoms that remain at varying concentrations are responsible for the differences in intensities observed at high q in the SANS data for samples at 1, 5, and 10 mg/mL exo-PS (**Figure 3**).

At low q values, the SANS data for the 10 mg/mL exo-PS in D_2O extend down to 0.001 Å^{-1} and exhibit a q-dependent intensity profile that reasonably matches the USANS data profile. This indicates the reliability of the desmearing process and underscores the consistency between the data collected for the sample in the two scattering regimes.

For q values below 0.003 Å^{-1}, the scattered intensities of the exo-PS samples display a q^{-n} dependency characteristic of mass fractals (refer to the Porod exponents in **Table S1**), with n falling within the range of 2 and 3. This suggests that the PS structure appears to be a repeating pattern that recurs at different levels of magnification. This trend is consistent with a branched polymer gel structure, featuring relatively large polymer clusters organized within a continuous network without discernible discrete cluster sizes.

The fitting of the 1 mg/mL exo-PS SANS data produced a correlation length of 48.9 ± 7.8 Å, which is approximately equivalent to the length of four M2 motifs (**Figure 4C**). While the presence of negatively charged glucuronic acid (GlcA) residues can lead to electrostatic repulsion and chain-swelling, the occurrence of the divalent cations such as Mg^{2+} and Ca^{2+} in the culture media could explain the cross-linking of GlcA residues [22]. The gelation of exo-PS contributes to the viscosity of the solutions and yields a relatively small correlation length[34].

For the 1 mg/mL exo-PS solution in the dilute regime, the fit to the SANS data generated a Porod exponent of 3.28 ± 0.16, which is inversely correlated to the Flory coefficient ($1/n \approx 0.3$). This estimated Flory coefficient value is typical of collapsed chains in water[32,35], as expected in the presence of divalent cation-mediated cross-linking[23,36]. The fits to the SANS profile for the 5 mg/mL exo-PS results in improved signal-to-noise data due to the higher PS concentration. Although the Porod exponent is slightly smaller, it remains closely aligned with the value expected for a mass fractal network.

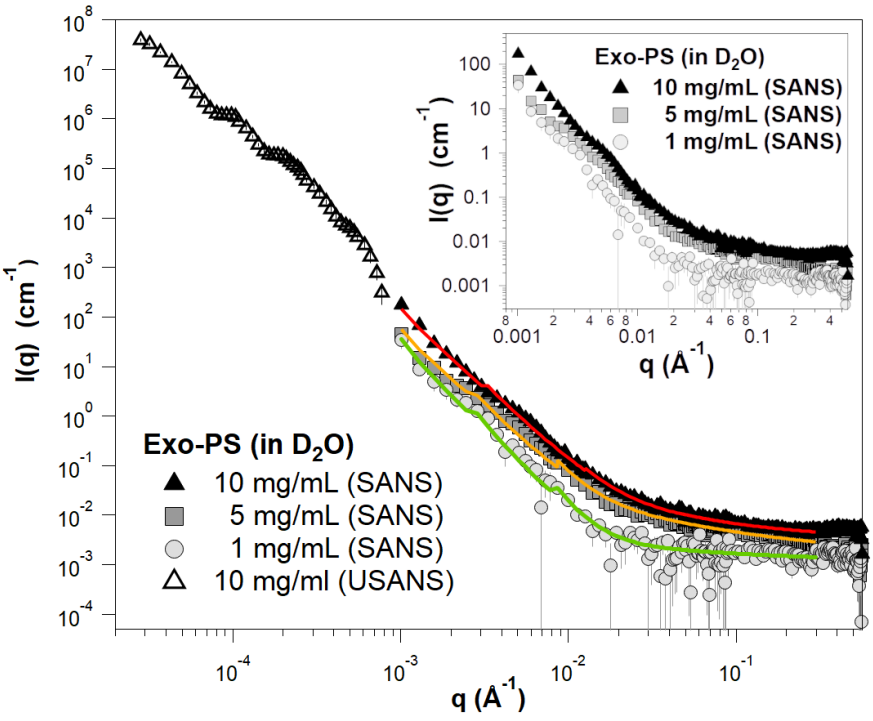

Figure 3. Background-subtracted, reduced SANS, and USANS data for the exo-PS solutions in D2O at varying concentrations. The USANS data shown has been desmeared using the macro-routines for Igor provided by the NCNR to account for the slit-smearing effects of the BT5 instrument on the experimental data. However, the desmeared USANS data were not utilized in the demonstrated data fits. The solid lines depict SANS data fits for the solutions at 1 mg/mL (green), 5 mg/mL (orange), and 10 mg/mL (red) exo-PS. The inset provides an enlarged view of the SANS data to highlight the distinctions observed between different concentrations. The error bars represent standard errors derived from counting statistics and, when not visibly discernible, are smaller than the corresponding data markers.

While there is no apparent change in the *q*-dependency of the scattered intensities for the 1 mg/mL exo-PS solution due to the poorer signal-to-noise ratio compared to the data collected at higher concentrations, clear changes in slope are evident at $q \approx 0.006$ Å^{-1} for the 5 mg/ml and 10 mg/mL solutions (**Figure 3** inset). These changes correspond to a transition from Porod scattering of PS clusters at lower *q*-values to a Lorentzian profile, which reflects the local structure of polysaccharide chains. At exo-PS concentrations of 5 and 10 mg/mL, an increase in inter-cluster interactions is reflected by the fitted Porod scales, which become larger at higher concentrations.

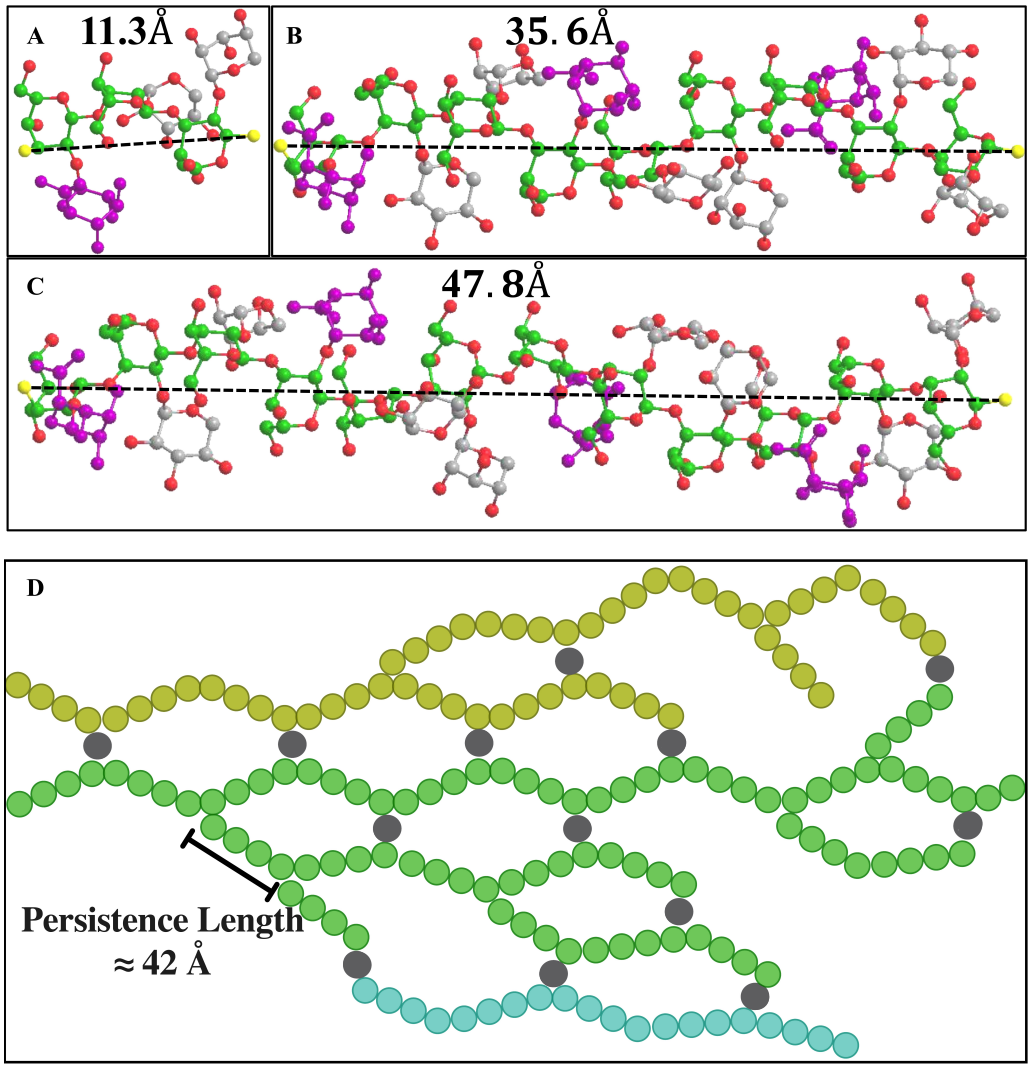

Figure 4. Schematic representation of M2 motif and exo-PS in water for one M2 (**A**), three M2 (**B**), and four M2 (**C**) repeating units, drawn and energy minimized using ChemDraw 22.2.0 and Chem3D 22.2.0, respectively. Mannoses are shown in green and glucuronic acids in purple. The distance between the two furthest oxygens (in yellow) that connect mannoses was measured to determine the approximate length of one (11.3 Å), three (35.6 Å), or four (47.8 Å) M2 units, respectively. (**D**) The cross-linking of exo-PS in water is represented, where each circle (except gray circles that represent divalent cations) represents one triad, and three chains are represented with different colors. A potential pattern of intra- and inter-chain crosslinking by the divalent

cations such as Mg^{2+} and Ca^{2+} (represented by gray circles) present in the cell culture media. The corresponding estimated persistence length (length of the region with rigid rod behavior) is approximately 42 Å. Image created with BioRender.com.

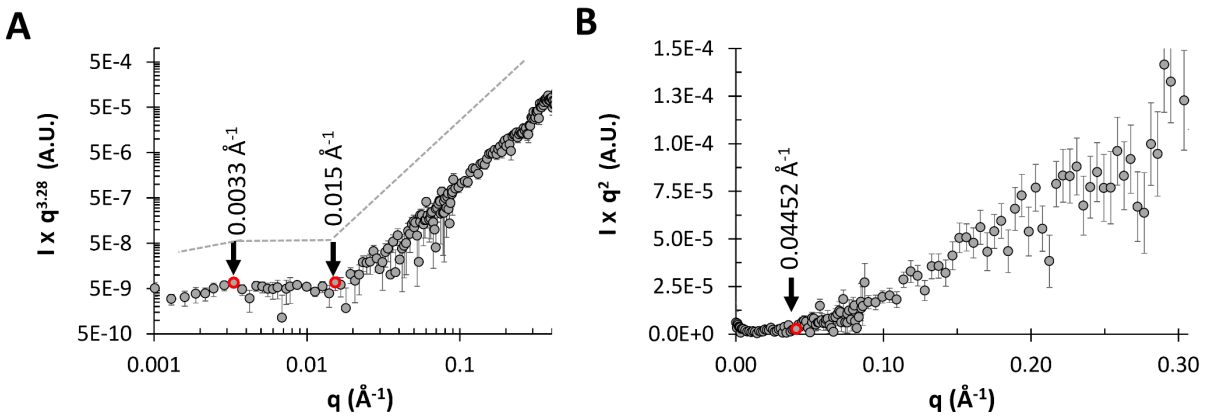

Figure 5. SANS data for 1 mg/mL exo-PS solution in D2O, are shown as (**A**) Porod exponent-weighted intensities and (**B**) a standard Kratky plot.

The q-dependency of the SANS intensity was shown at various length scales. The Porod region (**Figure 5A**) covers a q-range of ≈ 0.003-0.015 $Å^{-1}$, which corresponds to structural dimensions in the range of $(2\pi/q)$ ≈ 420-1900 Å. This is followed by the Lorentz region, characterized by a q-dependency of q^{-1}. The standard Kratky plot (**Figure 5B**) shows that at higher q ranges, the profile shifts at q^{*} ≈ 0.045 $Å^{-1}$, indicating a rigid rod behavior on a local scale. At this length scale, the PS chain is expected to exhibit rigid rod-like behavior without reorientation or branching [37,38]. The persistence length l can be calculated for an ideal Gaussian chain using the formula:

$$l = \frac{D}{q^*} \tag{3}$$

where D is a constant with a value of $6/\pi \approx 1.91$[38]. Applying this approximation to the exo-PS polymer in this local regime, the estimated persistence length is ≈ 42 Å. This length is consistent with that of three or four M2 units, suggesting a rigid rod-like behavior with no interactions between triads within each block.

Optical Microscopy, SANS, and USANS Analysis of Whole Fungal Cells. Figure 6 and **Table S2** present microscopy of *C. neoformans* H99 cells in different solutions. The microscopic images reveal a relatively high degree of variation in terms of both cell size and capsule thickness for the whole cell and gamma-irradiated cell suspensions. Without gamma irradiation, the average cell diameter was 13.9 ± 2.9 μm in D_2O and 13.2 ± 3.3 μm in H_2O, while cells subjected to gamma irradiation had an average cell diameter of 6.4 ± 2.7 μm in D_2O and 7.2 ± 2.9 μm in H_2O. The average capsule thickness before gamma-irradiation was also measured: 4.0 ± 1.4 μm in D_2O and 3.6 ± 1.5 μm in H_2O. Based on the microscopy data, the choice of solvents did not significantly affect cell di ameter or capsule thickness (unpaired t-test, $P > 0.05$, ns). However, gamma irradiation removed most of the capsular-PS (unpaired t-test, $P < 0.0001$, ****).

SANS and USANS data on whole and irradiated cells are presented in **Figure 7**, showing good agreement between the desmeared USANS data and the SANS data. In H_2O solutions, the incoherent scattering background dominates the intensity contributions at higher q in the SANS regime, and no differences are observed between whole and irradiated cell solutions. In D_2O solutions, a clear difference in the SANS profiles emerges at $q > 0.1$ Å^{-1}, where the M2 motif is expected to contribute towards scattering. In this specific region of the SANS profile, a lower plateau of scattering intensities is observed in gamma-irradiated samples. It is plausible that gamma irradiation disrupts the branching pattern correlations that SANS is typically sensitive to.

In the USANS regime, at $q < 0.00005$ Å^{-1}, all profiles exhibit a plateau in intensities roughly consistent with the sizes measured by microscopy. Given the high polydispersity of the samples, USANS data fitting was not attempted, as neutron scattering probes a significant amount of bulk sample compared to the images in **Figure 6**. Additionally, unknown contributions to the scattering profile from cellular components such as the nucleus or the cell wall further complicate data fitting.

The difference in size between whole and gamma-irradiated cells is apparent from the USANS profiles for both H_2O and D_2O samples, where the scattering profiles approach a plateau at the lowest measured q, as the intensities reach the Guinier regime. For non-irradiated samples, insufficient data points were collected to approximate the larger cell radii of gyration. Calculated radii of gyration for irradiated cell samples derived from Guinier data fit (**Figure S3** and **Table S3**) are consistent with the dimensions observed by optical microscopy.

Since exo-PS in H_2O solutions did not exhibit measurable contrast in the SANS regime, even at concentrations of 10 mg/mL, the discernible discrepancies in cell size between whole and gamma-irradiated cells in H_2O indicate differentiation between the exo-PS and capsular-PS. This is consistent with a gradient of PS densities in the pristine whole cells, ranging from an outer, more hydrated layer to an inner, denser layer closer to the cell wall, which is less solvent accessible and more resistant to ablation[21].

In the USANS data for H_2O solutions, there is an inflection point at $q \approx 0.0001$ Å^{-1} that is absent in the samples containing D_2O. Considering that no significant increase in polydispersity was detected by optical microscopy for the samples in D_2O compared to H_2O, the absence of inflection in D_2O solutions is not consistent with a resolution effect. Instead, the data may reflect a structural characteristic of the fungal cell body for which the solutions in H_2O provide better SLD contrast.

Given the complexity of the fungal cell and the unknown SLD of the different cell components, no specific structure or organelle can be objectively assigned to this area of the USANS profile.

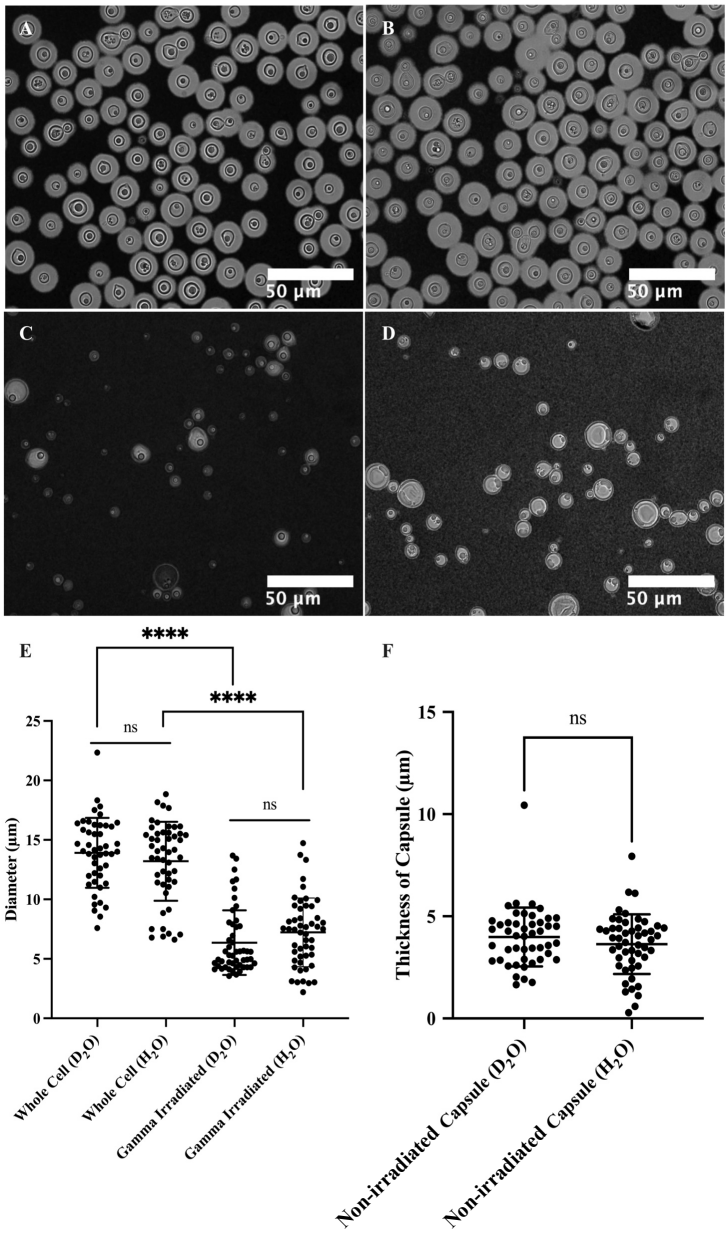

Figure 6. Microscopy of *C. neoformans* H99 cells in water and the effect of gamma irradiation on cellular and capsular dimensions. Samples were counterstained with India Ink particles, which are excluded by the dense PS capsule. Cells without gamma irradiation were resuspended in D_2O (**A**) and H_2O (**B**), and cells treated with 40 minutes of gamma irradiation were resuspended in D_2O (C)

and H_2O (**D**) as well. The cell diameters of all four samples were estimated (**E**), and capsule thickness for whole cells was obtained as the differences between the radii of cells and cell bodies (**F**). The t-test analyses are labeled based on their p-value ($p > 0.05$: ns; $p < 0.05$: *; $p < 0.01$: **; $p < 0.001$: ***; $p < 0.0001$: ****).

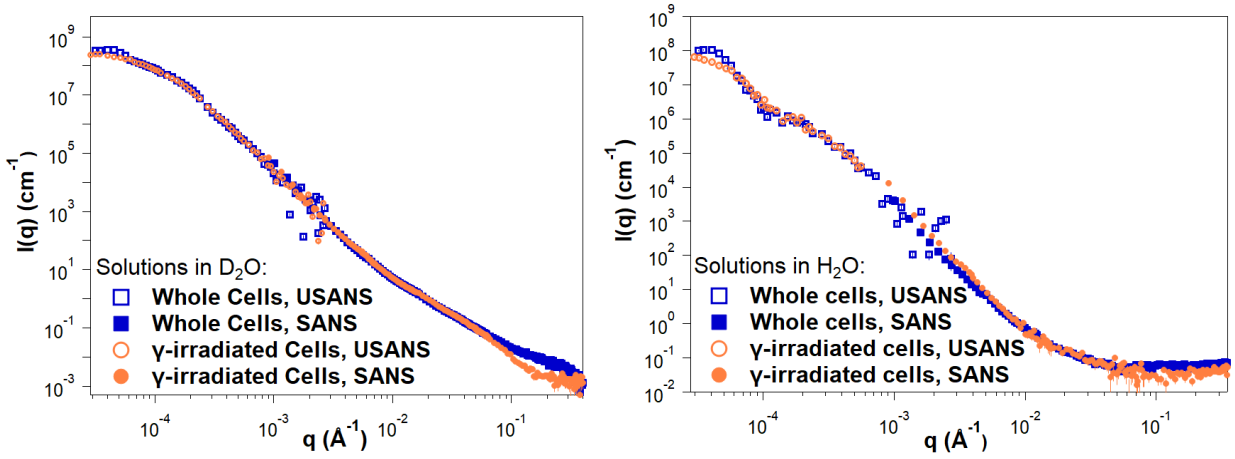

Figure 7. Reduced SANS (buffer subtracted) and USANS data collected for fungal cells in D_2O and H_2O solutions, for both intact and gamma-irradiated cells. The desmeared USANS data displayed compensates for the slit-smearing effects on the experimental data, allowing direct comparison with the SANS data for each sample. Error bars represent standard errors from counting statistics and are smaller than the corresponding data marker when not visible.

Fractal Analysis of Scanning Electron Micrographs. Image analysis of encapsulated whole cells and capsular structures reveals fractal patterns with dimensions ranging from 1.6 to 1.85 (**Figure 8**). Despite these samples undergoing dehydration during SEM processing and thus not being in their native state, the presence of fractal patterns in the polysaccharides is consistent with the neutron scattering data in solution. Moreover, this fractal pattern was observed even after

capsule dehydration and the coalescing of PS molecules into thick fibrils. This suggests a connection between the hydrated and dehydrated structures of polysaccharides, possibly reflecting the fungus's resistance to dehydrating conditions.

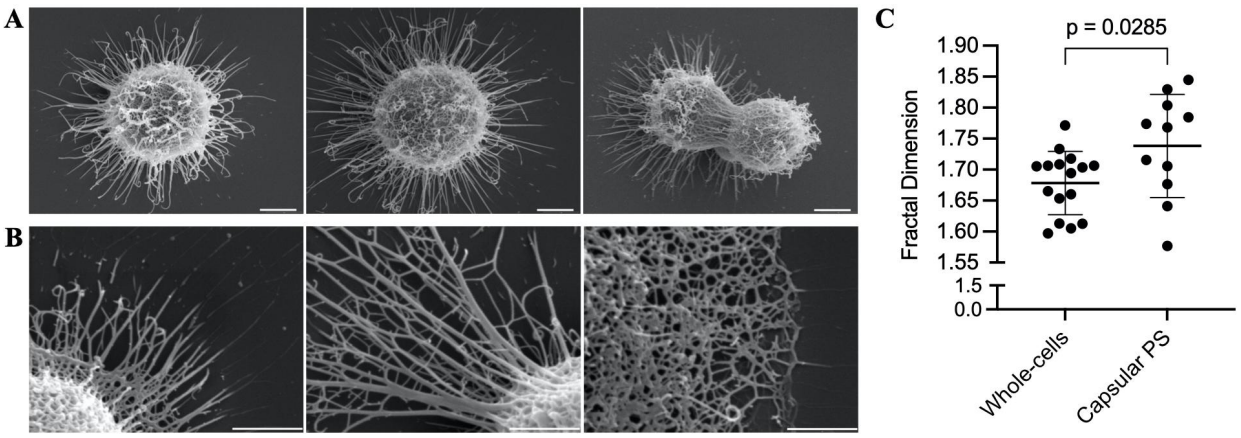

Figure 8. Fractal analysis of SEM micrographs of whole encapsulated cells and capsular-PS structures. (**A**) Representative whole encapsulated *C. neoformans* cells and (**B**) capsular-PS structures. Scale bars represent 2 and 1 micrometers, respectively. (**C**) Fractal dimensions of 27 micrographs were analyzed using the FracLac plugin in ImageJ.

CONCLUSIONS

This study demonstrates the effective use of neutron scattering and contrast variation techniques to gain insights into the structural characteristics of both *C. neoformans* exo-PS and cells under their native conditions. Our findings present compelling evidence that exo-PS inherently exhibits mass fractal characteristics, representing a self-similar branched system or network spanning a wide range of size scales. The SANS results from exo-PS scattering are consistent with a collapsed chain-like behavior stabilized by divalent cation bridges between negatively charged glucuronic acid residues, a phenomenon previously reported in the presence of water molecules[23].

Future SANS and USANS studies should address the concentration effects of exo-PS on hydrogen-to-deuterium exchange levels. High concentrations are likely to impact solvent accessibility to the polysaccharide, while lower concentrations may favor more uniformly chain-hydrated states and minimize scattering effects arising from overlapping and entanglement. The observed rigid rod behavior of exo-PS at local scales, with an estimated persistence length of approximately 42 Å, suggests that the arrangement of three to four GXM triads, particularly the M2 motif, involves short repeats where the chain direction may change at the end of each repeat, resulting in an overall semi-flexible structure. This local-scale rigidity of exo-PS agrees with molecular modeling studies, which propose that, at least within six GXM motifs, the ends of the chain do not bend into close proximity[39].

As a dominant virulence factor often targeted for antibody treatment, exo-PS plays a crucial role in infection. Recent research has identified decasaccharide (serotype A) as a possible minimal size for effective neutralizing mAb recognition, but our data offer a broader range of oligosaccharide sizes suitable for testing immune responses[40]. To better characterize the exo-PS secreted in humans during infection, similar studies on exo-PS secreted by isolated infecting fungal cells cultured in

media with the cation compositions of human fluids should be conducted to explore the effects of different types and concentrations of counterions.

It is important to note that sample preparation protocols can influence the measured structural properties, as previously suggested[10]. While this protocol can be used to reduce polydispersity and improve the scattering data resolution, it is important to note that the experimental data reflects only the structural features of the selected sample. Varying molar mass cutoffs during filtration can result in significant differences in the USANS regime (data not shown) and previous studies have shown that *C. neoformans* GXM fractions of different molar masses are functionally distinct[43]. Further work is needed to systematically characterize USANS and microscopy data for exo-PS chains representing the range of molar masses found *in vivo*.

Lastly, future SANS studies could utilize isotope-labeled dextrose or specific precursors to enhance the contributions of capsular-PS to the overall scattering profiles measured from whole cells, with the goal of further elucidating the differences between capsular-PS and exo-PS[10].

ASSOCIATED CONTENT

Supporting Information: **Figure S1**: dynamic light scattering data on the exo-PS sample; **Figure S2**: neutron scattering data on the exo-PS sample and data fitting; **Table S1**: fitting parameters for the exo-PS SANS data; **Table S2**: Cell dimensions; **Table S3**: Parameter fits to the USANS data for the gamma-irradiated cells; **Figure S3**: Guinier plots for the irradiated cell samples.

AUTHOR INFORMATION

Corresponding Author

*E-mail: rcorder4@jhu.edu.

* E-mail: susanat@udel.edu.

Author Contributions

RJBC and SCMT designed the neutron scattering experimental approach. CS and RJBC designed the cell culture and polysaccharide isolation protocols, prepared samples, and collected optical microscopy data. SCMT and CS collected and reduced the neutron scattering data. SCMT and ZW carried out the data fitting and analysis. AB carried out the fractal dimension analysis on SEM images. The manuscript was written through the contributions of all authors. All authors have approved the final version of the manuscript.

Notes

The authors declare no competing financial interest.

ACKNOWLEDGMENT

This work benefited from the use of the SasView application, originally developed under NSF award DMR-0520547. SasView contains code developed with funding from the European Union's Horizon 2020 research and innovation program under the SINE2020 project, grant agreement No 654000. SCMT is grateful for funding from the cooperative agreement #70NANB20H133 from NIST, U.S. Department of Commerce. We acknowledge the support of the National Institute of Standards and Technology, U.S. Department of Commerce, in providing the neutron research facilities used in this work. This work utilized facilities supported in part by the National Science Foundation under Agreement No. DMR-0944772. Certain commercial equipment, software, instruments, and materials are identified to foster understanding. Such identification does not imply recommendation or endorsement by the National Institute of Standards and Technology, nor does it imply that the materials or equipment identified are necessarily the best available for the purpose. The statements, findings, conclusions, and recommendations are those of the authors and do not necessarily reflect the view of NIST or the U.S. Department of Commerce. RJBC was supported by the Johns Hopkins University Center for AIDS Research (P30AI094189). The authors also thank Dr. Scott A. McConnell for reviewing the data and providing valuable input.

ABBREVIATIONS

PS, polysaccharide; GXM, Glucuronoxylomannans; SANS, small-angle neutron scattering; USANS, ultra-small-angle neutron scattering; SEM, scanning electron microscopy; SLD, scattering length density.

REFERENCES

(1) Rajasingham, R.; Smith, R. M.; Park, B. J.; Jarvis, J. N.; Govender, N. P.; Chiller, T. M.; Denning, D. W.; Loyse, A.; Boulware, D. R. Global Burden of Disease of HIV-Associated Cryptococcal Meningitis: An Updated Analysis. *Lancet Infect. Dis.* **2017**, *17* (8), 873–881. https://doi.org/10.1016/s1473-3099(17)30243-8.

(2) Ngan, N. T. T.; Flower, B.; Day, J. N. Treatment of Cryptococcal Meningitis: How Have We Got Here and Where Are We Going? *Drugs* **2022**, *82* (12), 1237–1249. https://doi.org/10.1007/s40265-022-01757-5.

(3) Pappas, P. G.; Perfect, J. R.; Cloud, G. A.; Larsen, R. A.; Pankey, G. A.; Lancaster, D. J.; Henderson, H.; Kauffman, C. A.; Haas, D. W.; Saccente, M.; Hamill, R. J.; Holloway, M. S.; Warren, R. M.; Dismukes, W. E. Cryptococcosis in Human Immunodeficiency Virus-Negative Patients in the Era of Effective Azole Therapy. *Clin. Infect. Dis.* **2001**, *33* (5), 690–699. https://doi.org/10.1086/322597.

(4); Casadevall, A.; Coelho, C.; Cordero, R. J. B.; Dragotakes, Q.; Jung, E.; Vij, R.; Wear, M. P. The Capsule of Cryptococcus Neoformans. *Virulence* **2019**, *10* (1), 822–831. https://doi.org/10.1080/21505594.2018.1431087.

(5) Maxson, M. E.; Cook, E.; Casadevall, A.; Zaragoza, O. The Volume and Hydration of the Cryptococcus Neoformans Polysaccharide Capsule. *Fungal Genet. Biol.* **2007**, *44* (3), 180–186. https://doi.org/10.1016/j.fgb.2006.07.010.

(6) Wear, M. P.; Hargett, A. A.; Kelly, J. E.; McConnell, S. A.; Crawford, C. J.; Freedberg, D. I.; Stark, R. E.; Casadevall, A. Lyophilization Induces Physicochemical Alterations in Cryptococcal Exopolysaccharide. *Carbohydr. Polym.* **2022**, *291*, 119547. https://doi.org/10.1016/j.carbpol.2022.119547.

(7) Cordero, R. J. B.; Pontes, B.; Frases, S.; Nakouzi, A. S.; Nimrichter, L.; Rodrigues, M. L.; Viana, N. B.; Casadevall, A. Antibody Binding to Cryptococcus Neoformans Impairs Budding by Altering Capsular Mechanical Properties. *J. Immunol.* **2013**, *190* (1), 317–323. https://doi.org/10.4049/jimmunol.1202324.

(8) Bowen, A.; Wear, M. P.; Cordero, R. J. B.; Oscarson, S.; Casadevall, A. A Monoclonal Antibody to Cryptococcus Neoformans Glucuronoxylomannan Manifests Hydrolytic Activity for Both Peptides and Polysaccharides*. *J. Biol. Chem.* **2017**, *292* (2), 417–434. https://doi.org/10.1074/jbc.m116.767582.

(9) Cordero, R. J. B.; Pontes, B.; Guimarães, A. J.; Martinez, L. R.; Rivera, J.; Fries, B. C.; Nimrichter, L.; Rodrigues, M. L.; Viana, N. B.; Casadevall, A. Chronological Aging Is Associated with Biophysical and Chemical Changes in the Capsule of Cryptococcus Neoformans. *Infect. Immun.* **2011**, *79* (12), 4990–5000. https://doi.org/10.1128/iai.05789-11.

(10) Frases, S.; Nimrichter, L.; Viana, N. B.; Nakouzi, A.; Casadevall, A. Cryptococcus Neoformans Capsular Polysaccharide and Exopolysaccharide Fractions Manifest Physical,

Chemical, and Antigenic Differences. *Eukaryot. cell* **2007**, *7* (2), 319–327. https://doi.org/10.1128/ec.00378-07.

(11) Frases, S.; Pontes, B.; Nimrichter, L.; Rodrigues, M. L.; Viana, N. B.; Casadevall, A. The Elastic Properties of the Cryptococcus Neoformans Capsule. *Biophys. J.* **2009**, *97* (4), 937–945. https://doi.org/10.1016/j.bpj.2009.04.043.

(12) Fonseca, F. L.; Nohara, L. L.; Cordero, R. J. B.; Frases, S.; Casadevall, A.; Almeida, I. C.; Nimrichter, L.; Rodrigues, M. L. Immunomodulatory Effects of Serotype B Glucuronoxylomannan from Cryptococcus Gattii Correlate with Polysaccharide Diameter. *Infect. Immun.* **2010**, *78* (9), 3861–3870. https://doi.org/10.1128/iai.00111-10.

(13) Cordero, R. J. B.; Frases, S.; Guimaräes, A. J.; Rivera, J.; Casadevall, A. Evidence for Branching in Cryptococcal Capsular Polysaccharides and Consequences on Its Biological Activity. *Mol. Microbiol.* **2011**, *79* (4), 1101–1117. https://doi.org/10.1111/j.1365-2958.2010.07511.x.

(14) Ellerbroek, P. M.; Lefeber, D. J.; Veghel, R. van; Scharringa, J.; Brouwer, E.; Gerwig, G. J.; Janbon, G.; Hoepelman, A. I. M.; Coenjaerts, F. E. J. O-Acetylation of Cryptococcal Capsular Glucuronoxylomannan Is Essential for Interference with Neutrophil Migration. *J. Immunol.* **2004**, *173* (12), 7513–7520. https://doi.org/10.4049/jimmunol.173.12.7513.

(15) Belay, T.; Cherniak, R.; Kozel, T. R.; Casadevall, A. Reactivity Patterns and Epitope Specificities of Anti-Cryptococcus Neoformans Monoclonal Antibodies by Enzyme-Linked Immunosorbent Assay and Dot Enzyme Assay. *Infect. Immun.* **1997**, *65* (2), 718–728. https://doi.org/10.1128/iai.65.2.718-728.1997.

(16) Frases, S.; Pontes, B.; Nimrichter, L.; Viana, N. B.; Rodrigues, M. L.; Casadevall, A. Capsule of Cryptococcus Neoformans Grows by Enlargement of Polysaccharide Molecules. *Proc. Natl. Acad. Sci.* **2009**, *106* (4), 1228–1233. https://doi.org/10.1073/pnas.0808995106.

(17) McFadden, D. C.; Fries, B. C.; Wang, F.; Casadevall, A. Capsule Structural Heterogeneity and Antigenic Variation in Cryptococcus Neoformans. *Eukaryot. Cell* **2007**, *6* (8), 1464–1473. https://doi.org/10.1128/ec.00162-07.

(18) Casadevall, A.; Nakouzi, A.; Crippa, P. R.; Eisner, M. Fungal Melanins Differ in Planar Stacking Distances. *PLoS ONE* **2012**, *7* (2), e30299. https://doi.org/10.1371/journal.pone.0030299.

(19) Cherniak, R.; Valafar, H.; Morris, L. C.; Valafar, F. Cryptococcus Neoformans Chemotyping by Quantitative Analysis of 1 H Nuclear Magnetic Resonance Spectra of Glucuronoxylomannans with a Computer-Simulated Artificial Neural Network. *Clin. Diagn. Lab. Immunol.* **1998**, *5* (2), 146–159. https://doi.org/10.1128/cdli.5.2.146-159.1998.

(20) Nakouzi, A.; Zhang, T.; Oscarson, S.; Casadevall, A. The Common Cryptococcus Neoformans Glucuronoxylomannan M2 Motif Elicits Non-Protective Antibodies. *Vaccine* **2009**, *27* (27), 3513–3518. https://doi.org/10.1016/j.vaccine.2009.03.089.

(21) Maxson, M. E.; Dadachova, E.; Casadevall, A.; Zaragoza, O. Radial Mass Density, Charge, and Epitope Distribution in the Cryptococcus Neoformans Capsule. *Eukaryot. Cell* **2007**, *6* (1), 95–109. https://doi.org/10.1128/ec.00306-06.

(22) Bryan, R. A.; Zaragoza, O.; Zhang, T.; Ortiz, G.; Casadevall, A.; Dadachova, E. Radiological Studies Reveal Radial Differences in the Architecture of the Polysaccharide Capsule

of Cryptococcus Neoformans. *Eukaryot. Cell* **2005**, *4* (2), 465–475. https://doi.org/10.1128/ec.4.2.465-475.2005.

(23) Nimrichter, L.; Frases, S.; Cinelli, L. P.; Viana, N. B.; Nakouzi, A.; Travassos, L. R.; Casadevall, A.; Rodrigues, M. L. Self-Aggregation of Cryptococcus Neoformans Capsular Glucuronoxylomannan Is Dependent on Divalent Cations. *Eukaryot. cell* **2007**, *6* (8), 1400–1410. https://doi.org/10.1128/ec.00122-07.

(24) Masuko, T.; Minami, A.; Iwasaki, N.; Majima, T.; Nishimura, S.-I.; Lee, Y. C. Carbohydrate Analysis by a Phenol–Sulfuric Acid Method in Microplate Format. *Anal. Biochem.* **2005**, *339* (1), 69–72. https://doi.org/10.1016/j.ab.2004.12.001.

(25) Ying, Q.; Chu, B. Overlap Concentration of Macromolecules in Solution. *Macromolecules* **1987**, *20* (2), 362–366. https://doi.org/10.1021/ma00168a023.

(26) Wagoner, T. B.; Çakır-Fuller, E.; Drake, M.; Foegeding, E. A. Sweetness Perception in Protein-Polysaccharide Beverages Is Not Explained by Viscosity or Critical Overlap Concentration. *Food Hydrocoll.* **2019**, *94*, 229–237. https://doi.org/10.1016/j.foodhyd.2019.03.010.

(27) Bercea, M.; Morariu, S.; Rusu, D. In Situ Gelation of Aqueous Solutions of Entangled Poly(Vinyl Alcohol). *Soft Matter* **2012**, *9* (4), 1244–1253. https://doi.org/10.1039/c2sm26094h.

(28) Hormnirun, P.; Sirivat, A.; Jamieson, A. M. Complex Formation between Hydroxypropylcellulose and Hexadecyltrimethylamonium Bromide as Studied by Light Scattering and Viscometry. *Polymer* **2000**, *41* (6), 2127–2132. https://doi.org/10.1016/s0032-3861(99)00415-2.

(29) Glinka, C. J.; Barker, J. G.; Hammouda, B.; Krueger, S.; Moyer, J. J.; Orts, W. J. The 30 m Small-Angle Neutron Scattering Instruments at the National Institute of Standards and Technology. *J. Appl. Crystallogr.* **1998**, *31* (3), 430–445. https://doi.org/10.1107/s0021889897017020.

(30) Barker, J. G.; Glinka, C. J.; Moyer, J. J.; Kim, M. H.; Drews, A. R.; Agamalian, M. Design and Performance of a Thermal-Neutron Double-Crystal Diffractometer for USANS at NIST. *J. Appl. Crystallogr.* **2005**, *38* (6), 1004–1011. https://doi.org/10.1107/s0021889805032103.

(31) Kline, S. R. Reduction and Analysis of SANS and USANS Data Using IGOR Pro. *J. Appl. Crystallogr.* **2006**, *39* (6), 895–900. https://doi.org/10.1107/s0021889806035059.

(32) Hammouda, B.; Ho, D. L.; Kline, S. Insight into Clustering in Poly(Ethylene Oxide) Solutions. *Macromolecules* **2004**, *37* (18), 6932–6937. https://doi.org/10.1021/ma049623d.

(33) Gilbert, E. P. Small-angle X-ray and Neutron Scattering in Food Colloids. *Current Opinion in Colloid & Interface Science* **2019**, *42*, 55-72. https://doi.org/10.1016/j.cocis.2019.03.005.

(34) Hyland, L. L.; Taraban, M. B.; Hammouda, B.; Yu, Y. B. Mutually Reinforced Multicomponent Polysaccharide Networks. *Biopolymers* **2011**, *95* (12), 840–851. https://doi.org/10.1002/bip.21687.

(35) Muller, F.; Manet, S.; Jean, B.; Chambat, G.; Boué, F.; Heux, L.; Cousin, F. SANS Measurements of Semiflexible Xyloglucan Polysaccharide Chains in Water Reveal Their Self-Avoiding Statistics. *Biomacromolecules* **2011**, *12* (9), 3330–3336. https://doi.org/10.1021/bm200881x.

(36) McFadden, D.; Zaragoza, O.; Casadevall, A. The Capsular Dynamics of Cryptococcus Neoformans. *Trends Microbiol*. **2006**, *14* (11), 497–505. https://doi.org/10.1016/j.tim.2006.09.003.

(37) Rosales, A. M.; Murnen, H. K.; Kline, S. R.; Zuckermann, R. N.; Segalman, R. A. Determination of the Persistence Length of Helical and Non-Helical Polypeptoids in Solution. *Soft Matter* **2012**, *8* (13), 3673–3680. https://doi.org/10.1039/c2sm07092h.

(38) Gupta, A. K.; Cotton, J. P.; Marchal, E.; Burchard, W.; Benoit, H. Persistence Length of Cellulose Tricarbanilate by Small-Angle Neutron Scattering. *Polymer* **1976**, *17* (5), 363–366. https://doi.org/10.1016/0032-3861(76)90228-7.

(39) Kuttel, M. M.; Casadevall, A.; Oscarson, S. Cryptococcus Neoformans Capsular GXM Conformation and Epitope Presentation: A Molecular Modelling Study. *Molecules* **2020**, *25* (11), 2651. https://doi.org/10.3390/molecules25112651.

(40) Guazzelli, L.; Crawford, C. J.; Ulc, R.; Bowen, A.; McCabe, O.; Jedlicka, A. J.; Wear, M. P.; Casadevall, A.; Oscarson, S. A Synthetic Glycan Array Containing Cryptococcus Neoformans Glucuronoxylomannan Capsular Polysaccharide Fragments Allows the Mapping of Protective Epitopes. *Chem. Sci*. **2020**, *11* (34), 9209–9217. https://doi.org/10.1039/d0sc01249a.

(41) Albuquerque, P. C.; Fonseca, F. L.; Dutra, F. F.; Bozza, M. T.; Frases, S.; Casadevall, A.; Rodrigues, M. L. Cryptococcus Neoformans Glucuronoxylomannan Fractions of Different Molecular Masses Are Functionally Distinct. *Futur. Microbiol*. **2014**, *9* (2), 147–161. https://doi.org/10.2217/fmb.13.163.